Appl. Phys. A 89, 933–940 (2007)
DOI: 10.1007/s00339-007-4288-y

Applied Physics A
Materials Science & Processing

I. MAROZAU[1]
M. DÖBELI[2]
T. LIPPERT[1,✉]
D. LOGVINOVICH[3]
M. MALLEPELL[2]
A. SHKABKO[3]
A. WEIDENKAFF[3]
A. WOKAUN[1]

One-step preparation of N-doped strontium titanate films by pulsed laser deposition

[1] Paul Scherrer Institut, 5232 Villigen PSI, Switzerland
[2] Ion Beam Physics, Paul Scherrer Institut and ETH Zurich, 8093 Zurich, Switzerland
[3] Empa, Überlandstrasse 129, 8600 Dübendorf, Switzerland

Received: 25 June 2007 / Accepted: 17 August 2007
Published online: 28 September 2007 •

ABSTRACT Perovskite-type oxynitrides exhibit promising electrical and optical properties and can possibly be used in the future as functional materials for electrical, photo-, and electrochemical applications. Continuous heterovalent substitution of oxygen ions by nitrogen ions allows tuning of the desired optical and/or electronic properties to the application specifications. In the present work deposition of $SrTiO_3$:N films by pulsed reactive crossed beam laser ablation was studied in order to examine the influence of different deposition parameters on the film crystallinity and composition. The deposited films exhibit a perovskite-type crystal structure and reveals epitaxial growth on MgO(100) substrates. The unit cell parameters of the deposited $SrTiO_3$:N films range within $3.911 < a < 3.919$, which is slightly larger than for polycrystalline $SrTiO_3$ ($a = 3.905$). The studied films reveal an oxygen content in the range of $(2.70 - 2.98) \pm 0.15$. The relative N content (vs. O) can be tuned within the range of 1.0%–3.0% by adjusting the deposition parameters. The N : O concentration ratio increases with increasing laser fluence and target-to-substrate distances, while the substrate temperature has a more complex influence on the nitrogen concentration. In the range of 580–650 °C the [N]/[O] ratio increases while further heating results in a gradual decrease of the N content.

PACS 81.15.Fg; 68.55.-a; 81.05.Zx

1 Introduction

Perovskite-type materials attract great interest due to varieties of their properties and applications [1, 2]. The most common way to tune the material properties is substitution of atoms in the perovskite crystal structure. While most research efforts on perovskite-type oxides have been focused on modifications of the cation composition [2], a less explored approach was to investigate modifications of the anion composition. However, anionic substitution provides an additional alternative possibility for modification and improvement of the properties [3]. Nitrogen is one potential candidate for replacement of oxygen in oxides, due to the similar ionic radii and electronic structures of both anions. Partial substitution of O with N in perovskites yields perovskite-type oxynitrides [3–5]. The new materials exhibit promising electrical and optical properties, which can be potentially tuned by continuous substitution of O with N [3, 6–10]. Perovskite-type oxynitrides were proposed as potential non-toxic inorganic pigments to replace currently used materials containing lead and other heavy metals [8, 11]. In the $Ca_{1-x}La_xTiO_{3-x}N_x$ system the band gap energy (which determines the absorption edge position, i.e. the colour) can be adjusted within the range of $2.2 < E_{bg} < 3.7$ by modification of the nitrogen content [12]. $BaTaO_2N$ and $SrTaO_2N$ were shown to have high bulk dielectric permittivities in excess of 2500 [5].

Substitution of divalent oxygen anions with trivalent nitrogen anions leads to an increase of the formal charge in the anionic sublattice. To keep the necessary neutral valence, four main different possibilities exist:

1. Cationic substitutions with cations having higher oxidation states can be used to compensate the anionic negative charge increase [9, 12]:

$$ATiO_3 \Rightarrow A_{1-x}La_xTiO_{3-x}N_x \ (A = Ca, Sr, Ba)\,. \qquad (1)$$

   In this particular case, the amount of incorporated nitrogen is governed by the degree of cationic substitution, yielding an easy control over the nitrogen content.
2. Charge compensation can also be carried out by anionic vacancies formation [13, 14]:

$$ATiO_3 \Rightarrow ATiO_{3-3x/2}N_x \ (A = Sr, Ba)\,. \qquad (2)$$

   This type of charge compensation is favourable in crystal structures, which are "tolerant" for anionic vacancies and/or if any other compensation mechanisms are non-relevant.
3. An increase of the anionic formal charge due to the nitrogen incorporation may result in an increase of the transition metal oxidation state [4, 7]:

$$\overset{+4}{Sr}\overset{+4}{Mo}O_3 \Rightarrow Sr\ \overset{+4,+5}{Mo}\ O_{3-x}N_x\,. \qquad (3)$$

   This mechanism indicates a specific feature of nitrogen to stabilise the higher oxidation states of transition metals.
4. Finally, substitution of oxygen with nitrogen can result in changes of the crystal structure. This approach can be used

✉ Fax: +41-56310-2688, E-mail: thomas.lippert@psi.ch

for synthesis of new oxynitride perovskite-type phases starting from non-perovskite oxide precursors [3, 10]:

$$SrMoO_4 \Rightarrow SrMoO_{3-x}N_x\,. \quad (4)$$

For many applications as well as for certain studies it is indispensable to produce thin films [15]. Oxynitride films can be prepared by two different approaches. The first approach is a two-step process, which implies deposition of the oxide film precursor and its subsequent thermal or plasma ammonolysis [16]. The second approach is the direct deposition of the oxynitride film in one step. The most widely used method is RF-magnetron sputtering with a reactive nitrogen plasma [17, 18]. However, this technique does not allow deposition of epitaxial films [17, 18]. Another method for the one-step deposition of oxynitrides films is pulsed laser deposition (PLD). This method allows preparation of films with complex compositions [19, 20]. In our work we study the applicability of PLD for the preparation of high quality epitaxial perovskite-type oxynitride thin films.

Titanates were chosen as model systems to investigate the influence of different deposition parameters on the crystal structure, chemical composition, and properties of the studied films. Alkaline earth titanates form corresponding oxynitrides after thermal or plasma ammonolysis [13, 14]. The resulting oxynitrides may have possible applications as photocatalysts [21], pigments [9], or dielectric materials for capacitors [13].

This paper is focused on the investigation of the influence of different deposition parameters on the crystallinity, microstructure and composition of the nitrogen-doped strontium titanate films prepared by PLD.

2 Experimental

2.1 *Film deposition*

Nitrogen-doped strontium titanate ($SrTiO_3$:N) films were prepared by pulsed reactive crossed beam laser ablation (PRCLA). This technique is a variant of PLD, which utilises a pulsed gas source synchronized with the laser used for ablating the target material [22–28]. The gas pulse crosses the ablation plume close to its origin. This geometry provides a high number of gas phase interactions between the ablated plasma species and molecules from the gas pulse [22]. This results in a higher plasma ionisation degree and an increased amount of the reactive anionic species, which are formed by collisions of the gas pulse molecules with the ablated plasma species. Therefore, this modification of conventional PLD allows a better control of the anionic composition of growing film by choosing an appropriate gas for the gas pulse [25, 29]. This could play an especially important role for deposition of thin films with controlled anion stoichiometry, e.g. in the case of oxynitride materials. In our studies we applied a nitrogen gas pulse coupled with a nitrogen background for deposition of $SrTiO_3$:N films.

A KrF excimer laser ($\lambda = 248$ nm) was used at a repetition rate of 10 Hz. All studied films were deposited on MgO(100) substrates (1.0 cm by 1.0 cm). Several sample series were prepared to study the influence of different PLD parameters. One set of deposition parameters was chosen as the standard condition for comparison. In every sample series only one of these standard parameters is varied systematically, while the others are kept constant. The reference film was deposited at a laser fluence (F) of 5.0 J cm^{-2}. The rod-shaped ceramic $SrTiO_3$ target was located at a distance of 5.0 cm from the substrate, which was heated to 650 °C. Two gas sources were used during film growth: a leak valve to provide a background pressure of nitrogen (8.0×10^{-2} Pa) and a nitrogen gas pulse, synchronised with the laser (pulse length 400 μs, feed pressure 2.0×10^5 Pa). More experimental details about PRCLA can be found elsewhere [22, 23].

The influence of the following PLD parameters on the film properties was studied:

1. Laser fluence, ranging from 2.0 to 6.0 J cm^{-2};
2. Target-to-substrate ($d_{T\text{–}S}$) distance, 3.0–5.0 cm;
3. Substrate temperature (T_S), 580–720 °C;
4. Background gas and gas pulse (nitrogen and oxygen in different combinations).

2.2 *Film characterisation*

The film crystallinity was studied by X-ray diffraction analysis (XRD) using a Siemens D5000 diffractometer in the standard $\Theta - 2\Theta$ mode (Cu K_α irradiation, 2Θ range of 20–80°, step 0.005°, 0.3 s/step). The cubic unit cell parameters were determined from the position of the (200) film reflections. Only the (200) reflections could be used, because the intensities all other film reflections are too small to be applied for the estimation of the lattice constants. To confirm the phase composition grazing incidence X-ray diffraction measurements of some samples were performed on a Phillips X'Pert diffractometer (Cu K_α irradiation, incident angle of 1°, 2Θ range of 10–100°, step 0.05°, 0.5 s/step).

The film thickness was measured by a Dektak 8 profilometer (tip size of 5 μm, scanning force 3 μg, scanning speed 150 μm s^{-1}) and calculated from the Rutherford backscattering data analysis. The film roughness was calculated from the profilometry data. Prior to calculations, the initial data were filtered to remove the waviness contribution by applying a cut-off filter with a wavelength of 100 μm [30]. Then, the root-mean-square roughness was calculated for a film profile, where no particles were observed.

The chemical composition of studied films (Sr : Ti : O concentration ratio) was determined by Rutherford backscattering spectrometry (RBS) [31]. The measurements were performed using a 2 MeV ^{4}He ion beam and a silicon surface barrier detector under 165°. The collected RBS data were simulated with the RUMP software [32]. The experimental uncertainty in cations and oxygen stoichiometry, determined by RBS, is ±3% and ±5%, respectively. The N : O concentration ratio was obtained from elastic recoil detection analysis (ERDA). For the measurements a 12 MeV ^{127}I beam was used under an 18° incident angle. The scattered recoils were identified by the combination of a time-of-flight spectrometer with a gas ionisation chamber. The experimental uncertainty in determination of the N : O concentration ratio by ERDA is ±0.005. For the reference film (deposited at a laser fluence of 5.0 J cm^{-2}, $d_{T\text{–}S} = 5.0$ cm and $T_S = 650$ °C), a detailed depth-profiling ERDA analysis was performed. The concentration of

each element in the film was analysed as a function of depth in the range of 0–185 nm.

3 Result and discussion

3.1 *General aspects of film deposition*

The most probable mechanism of anionic charge compensation in N-doped strontium titanate is the formation of anionic vacancies (2), as no simultaneous substitutions in the cationic sublattices occur, and titanium is already present in the highest possible oxidation state of +4. This situation is comparable to that in the case of N-doped barium titanate, where the charge compensation also occurs via formation of oxygen ion vacancies [14].

Pulsed laser deposition of oxides in a high vacuum typically results in the formation of oxygen-deficient films [33, 34], because the light oxygen species (atoms and ions) have a lower sticking probability and a higher scattering degree in the ablation plasma plume, compared to the heavier cationic species. Thus, deposition of oxide films by PLD requires an additional source(s) of O to achieve deposition of films without oxygen deficiencies. The most commonly used sources of O are the background gas [20, 34], a gas pulse (PRCLA) [26, 29], and a RF-induced plasma plume (RF-plasma assisted PLD) [35]. In our experiments the growing strontium titanate films are expected to contain anionic vacancies as no additional sources of O are used [33]. In the presence of reactive nitrogen species in the plasma these vacancies can be occupied by N atoms resulting in the formation of an oxynitride phase. This is in agreement with the mechanism of oxynitride formation in the thermal ammonolysis process, where partial reduction of the oxide precursor precedes incorporation of nitrogen into the crystal lattice [10].

3.2 *Film thickness and roughness*

The film thicknesses (d) were measured by a profilometer and calculated from the combination of RBS data analysis and the unit cell parameters, using the following equation:

$$d = \left(\frac{n_{\mathrm{M}}}{S}\right) a^3 , \tag{5}$$

where (n_{M}/S) is the film thickness in molecules per cm^2 obtained from RBS; a is the unit cell parameter calculated from XRD data. The results of these calculations for a series of films, deposited at different laser fluences at constant $T_{\mathrm{S}} =$ 650 °C and $d_{\mathrm{T\text{–}S}} = 5.0$ cm, are shown in Fig. 1a together with the measured thicknesses. Both methods give similar values, suggesting good measurement accuracy. The film thicknesses increase with increasing laser fluence due to the higher target ablation rate [24]. Figure 1b shows the comparison of fluence dependencies of the ablation rate (measured on the 93% dense polycrystalline $SrTiO_3$ target used for PRCLA) vs. the deposition rate (calculated from the film thickness assuming 100% dense films). Both the ablation and the deposition rates increase continuously with increasing the laser fluence up to 8 J cm^{-2}. The ratio between the deposition and the ablation rates (transport factor) is $\sim 1\%$ and has a minor fluence dependence (insert in Fig. 1b). This suggests that within the studied laser fluence range, the material transport from the target to the substrate is essentially independent on the laser fluence. A small transport factor of $\sim 1\%$ indicates that most of the ablated material is lost during the deposition due to the small size of the substrate compared to the ablation plume volume at the target-to-substrate distance of 5 cm and scattering of the ablated species by collisions in the gas phase during the material transport from the target to the substrate. Figure 2a shows the changes of the film thickness as a function of the target-to-substrate distance. The decrease of the thicknesses with increasing $d_{\mathrm{T\text{–}S}}$ is due to the higher degree of plasma scattering, which results in a smaller amount of the ablated target material arriving at the substrate [24]. As a result, the deposition rate and therefore the film thickness decrease with increasing target-to-substrate distance. No influence of the substrate temperature on the film thicknesses was found within the studied temperature range of 580–720 °C (Fig. 2b).

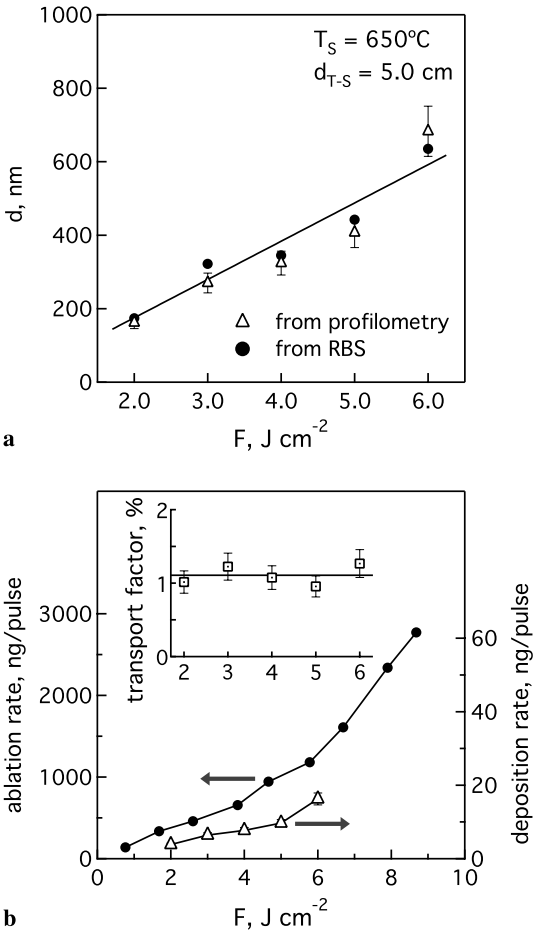

FIGURE 1 (**a**) Variation of the film thickness vs. the laser fluence. (**b**) Comparison of fluence dependencies of the ablation rate measured on the 93% dense polycrystalline $SrTiO_3$ target vs. the deposition rate of N-doped $SrTiO_3$ films calculated from the film thickness assuming 100% dense films. The *insert* shows variations of the transport factor (ratio between the deposition and the ablation rates) with the laser fluence

The film roughness as a function of substrate temperature is shown in Fig. 3. The roughness tends to increase with increasing substrate temperature. Deposition at higher temperatures results in a higher mobility of atoms, ions and clusters at the substrate surface, which may lead to the formation of larger crystallites at the surface of a growing film. There-

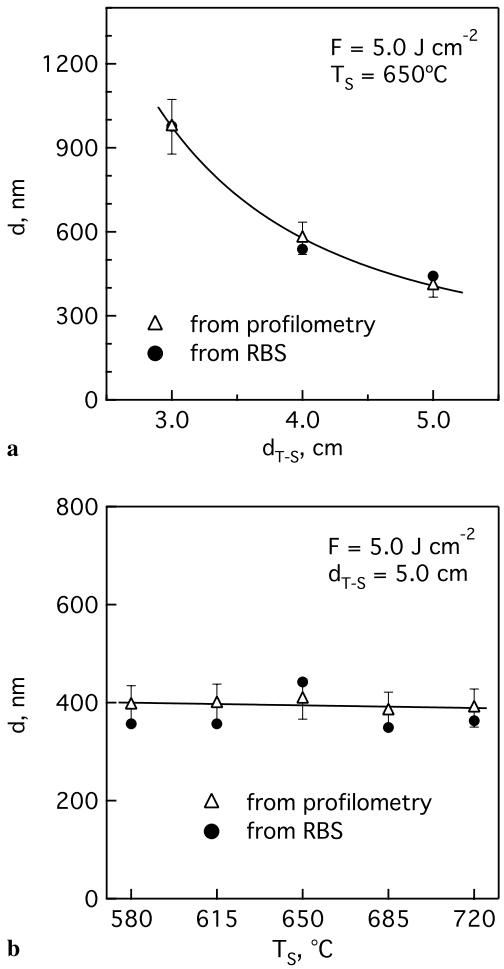

FIGURE 2 Thickness of $SrTiO_3$:N films as a function of target-to-substrate distance (**a**), and substrate temperature (**b**)

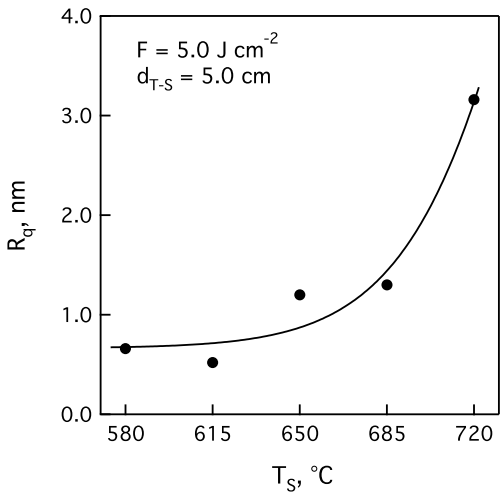

FIGURE 3 Substrate temperature dependence of the root-mean-square roughness of N-doped $SrTiO_3$ films calculated from the profilometry data

fore the films, grown at higher substrate temperatures, exhibit larger surface topographic features and higher roughness. The influence of other studied deposition parameters on the film roughness is less pronounced. Films grown at different laser fluences and target-to-substrate distances exhibit a roughness in the range of 0.83–1.41 nm, depending mainly on the homogeneity of the substrate heating. A relatively low roughness of 0.56 nm is achieved for the films grown at the lowest laser fluence of 2 J cm^{-2}, which can be explained by the significantly lower film thickness.

3.3 *Film composition*

The chemical composition of the films was determined in two steps. First, RBS measurements were performed to obtain the Sr : Ti : O stoichiometry. However, the sensitivity of RBS for light elements is relatively poor [31], therefore, ERDA was performed to obtain the N concentration. The utilisation of a substrate (MgO) with only light elements results in a smaller uncertainty of RBS data analysis [31]. An example of a RBS spectrum including the fitting is presented in Fig. 4a. A small barium contamination ($\sim 0.5\%$ vs. Sr concentration) is found in all samples. This contamination originates from the $SrTiO_3$ target, which has been confirmed by laser ablation inductively coupled plasma mass spectrometry (LA-ICP-MS) of the target material. The physico-chemical properties

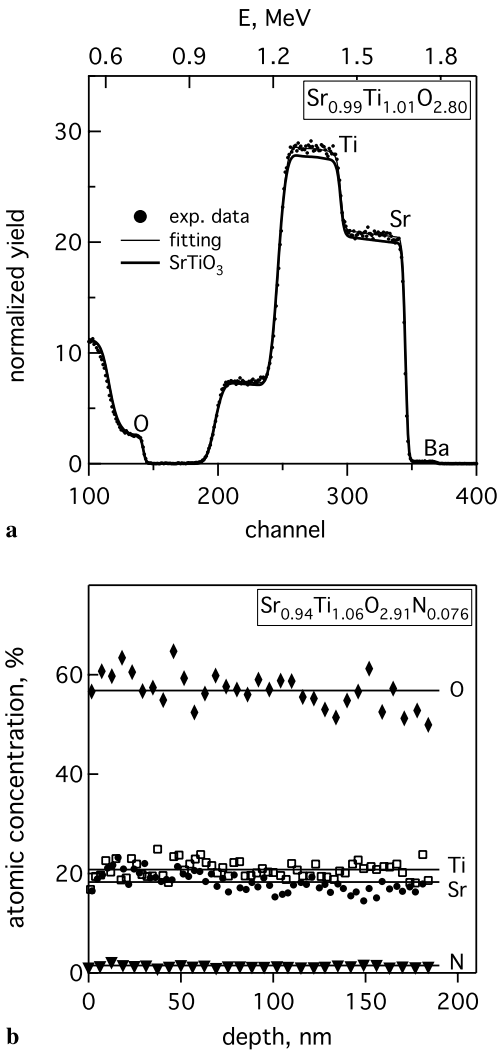

FIGURE 4 Chemical composition of the reference film (deposited at a laser fluence of 5.0 J cm^{-2}, $d_{T\text{–}S} = 5.0$ cm and $T_S = 650\,^{\circ}$C) by (**a**) RBS analysis and (**b**) ERDA depth profiling analysis. The simulated RBS spectrum of stoichiometric $SrTiO_3$ is included

of Ba^{2+} are very similar to those of Sr^{2+} [36]. Thus, a minor amount of barium acts as an isovalent dopand in the A-site of $SrTiO_3$ and has most probably a minor influence on the crystal structure and properties of the grown films. The RBS analysis confirms also a stoichiometric transport of the cations from the target to the growing films. The difference between the Sr and Ti content in the films is small and is within the limit of experimental uncertainty.

The oxygen content ([O]), determined by RBS, typically lies in the range $2.75 < [O] < 2.98 \pm 0.15$. The lowest O concentration of 2.70 ± 0.15 was detected in the sample deposited at the shortest target-to-substrate distance of 3.0 cm, which could be due to an increased probability of resputtering of light elements, such as O (and N), at low target-to-substrate distances by plasma species with high kinetic energies [37]. The observed values of oxygen content in the studied films are very close to the ideal stoichiometry value for 3-dimensional perovskites of 3. This is rather remarkable, as the only oxygen source used during deposition is the target, and normally an additional source(s) of oxygen must be supplied to achieve almost ideal oxygen contents in the oxide films deposited by PLD, or to achieve a pure perovskite phase at all [26, 29, 34, 35]. The oxygen content in the studied films is higher compared to the reported value of 2.50 in the strontium titanate films, deposited by PLD at a base pressure of $< 10^{-5}$ Pa, while deposition with an oxygen background pressure of 50 Pa results in less oxygen-deficient films ([O] = 2.95) [33]. This is different to the classical synthesis of titanates in air or oxygen atmosphere, where titanates with ideal stoichiometric oxygen content are usually obtained (i.e. $SrTiO_3$). Previous investigations have shown, that cobaltate and manganate perovskite-type films, prepared by PRCLA using two oxygen sources (N_2O for the gas pulse and O_2 as the background), can exhibit relatively high oxygen deficiencies of up to $\delta = 0.6$ [26, 29]. Most of the films, studied in this work, were deposited using N_2 for the gas pulse and as background gas, i.e. no oxidizing source was used. The high oxygen content in the $SrTiO_3$:N films is therefore prominent and not yet fully understood, as the sticking probability and scattering degree of oxygen should not be influenced too strongly by using N_2 as background gas compared to O_2. This unambiguously suggests that the oxygen content in films, prepared by PLD, is strongly influenced by the nature of the applied material in addition to the deposition parameters as reported elsewhere [24, 29].

The nitrogen content ([N]) in the prepared $SrTiO_3$:N films was determined by ERDA and normalized to the oxygen content. Figure 5 presents the relative N concentration as a function of different deposition parameters. The nitrogen-to-oxygen concentration ratio ([N]/[O]) increases with the laser fluence, reaching a maximum value of 0.030 ± 0.005 at a laser fluence of 6.0 J cm^{-2}, which corresponds to a nitrogen content of $Sr_{1.02}Ti_{0.98}O_{2.95}N_{0.089}$ (Fig. 5a). The probability of incorporation of N species in the film arriving at the heated substrate depends mainly on their chemical reactivity and the substrate temperature, although other parameters such as the presence of oxygen species also have an influence. Higher laser fluences result in higher ablation rates, kinetic energies, and plasma ionisation degrees, which leads to a higher reactivity of the nitrogen species, e.g. by formation of N or N* by collisions of the energetic plasma species with N_2 molecules from the gas pulse and background [22]. This results in an increase of the relative N concentration in the films with increasing laser fluence. The variation of the nitrogen content vs. the substrate temperature is presented in Fig. 5b. The nitrogen content increases for T_S between 615 and 650 °C and decreases slightly upon further heating. The sudden increase of the relative N concentration could be associated with an enhanced kinetics of the oxynitride phase formation due to a higher surface mobility and bulk diffusion

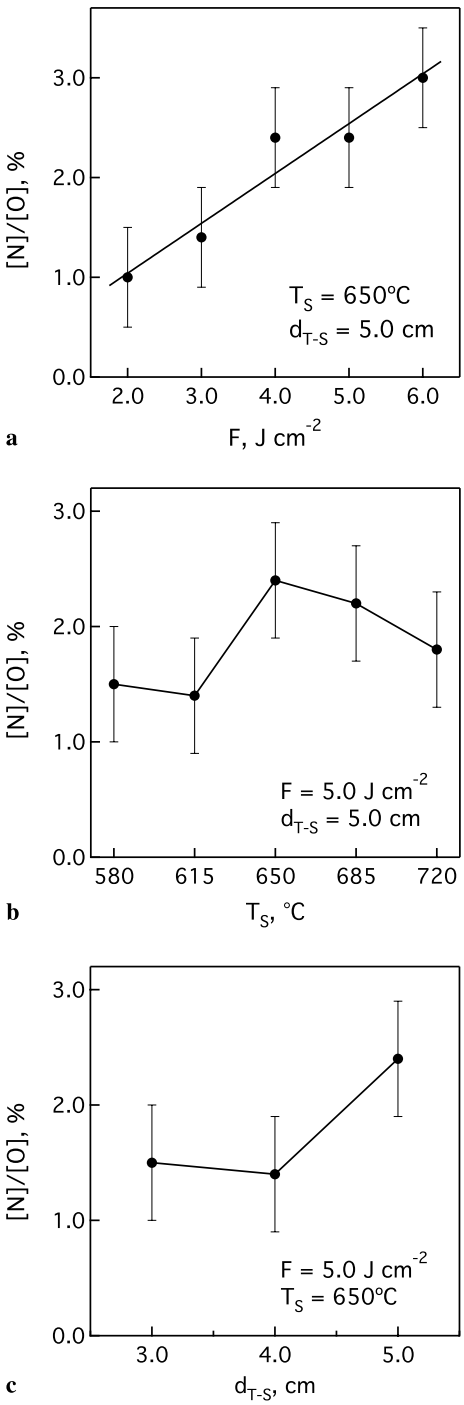

FIGURE 5 Variations of the relative nitrogen content in the films vs. the laser fluence (**a**), substrate temperature (**b**), and target-to-substrate distance (**c**)

of the reactive nitrogen species from the plasma at the substrate surface [24]. Further heating, above $T \sim 650\,^{\circ}\mathrm{C}$, results in a gradual decrease of incorporated nitrogen due to the lower thermodynamical stability of the oxynitride phase compared to the oxide [3]. This can also be related to the lower sticking probability of the lighter N species compared to oxygen. In Fig. 5c the relative nitrogen concentration is shown as a function of the target-to-substrate distance. The nitrogen content has a tendency to increase with increasing $d_{\mathrm{T\text{–}S}}$. Most probably this originates from a preferential resputtering of lattice nitrogen by the plasma at lower target-to-substrate distances, where the arriving plasma species have higher kinetic energies [38]. This may be due to the lower sticking probability of N compared to O or due to thermodynamical reasons (resputtering of N atoms from the growing film in the form of very stable N_2 molecules).

It is noteworthy to mention, that the highest N : O concentration ratio of 3.0% among the studied $SrTiO_3$:N films is very close to the value of $\sim 3.5\%$ obtained for another N-doped alkaline earth titanate – $BaTiO_3$:N, prepared by thermal ammonolysis at 950 °C [14].

Depth-profiling analysis of ERDA data was performed for the reference film (deposited at a laser fluence of $5.0\,\mathrm{J\,cm^{-2}}$, $d_{\mathrm{T\text{–}S}} = 5.0$ cm and $T_{\mathrm{S}} = 650\,^{\circ}\mathrm{C}$). The atomic concentration of each element was analysed as a function of the depth in the range of 0–185 nm. The results of this analysis are presented in Fig. 4b. No changes in the concentration of cations were detected within the studied depth range. The depth profile of the N content in the film is almost flat, indicating that no essential re-exchange of the incorporated N with O from air occurs at the film surface upon its storage at room temperature. The analysis of the oxygen concentration in the film shows that the O content is higher at the film surface region and lower in the bulk of the film. This originates most probably from an oxygen uptake by the anion-deficient $SrTiO_3$:N phase, which occurs at the film surface. The averaged film composition, obtained from the ERDA depth profiling data over the range of 0–185 nm is $Sr_{0.94}Ti_{1.06}O_{2.91}N_{0.076}$, which is in good agreement with the RBS analysis, i.e. $Sr_{0.99}Ti_{1.01}O_{2.80}$ over the film thickness of ~ 440 nm, of the same film (Fig. 4a). The slightly higher oxygen content (compared to the RBS results) may originate from the smaller analytical depth of ERDA, where the high O concentration at the film surface results in a higher overall oxygen content. However, the difference in the O content obtained from RBS and ERDA analyses is small and is within the limits of experimental uncertainty.

Two films were also prepared where N_2 was replaced by O_2, either in the gas pulse or in the background to study the influence of the presence of an oxidizing source on the nitrogen content (i.e. one film was prepared with N_2 in the gas pulse and in O_2 background while another one with O_2 in the gas pulse and in N_2 background). For both samples no N could be detected by ERDA in the films. This is in agreement with theoretical estimations, which predict that at high temperatures in oxidizing atmosphere (i.e. in the presence of oxygen) the formation of the oxide phase is thermodynamically much more favourable than the formation of an oxynitride due to the high stability of N_2 [3].

A control of the composition by deposition parameters in PLD allows the deposition of films with desired N and O contents (within the certain limits, e.g. $SrTiO_{2.70-2.98}N_{0.030-0.089}$). This is the basis for an understanding of the influence of the N content and the possible oxygen deficiency on the properties of oxynitrides films, such as color, conductivity, band gap energy, dielectric permittivity, etc.

3.4 *Structural characterisation of* $SrTiO_3$*:*N *films. Film crystallinity and unit cell parameters*

Figure 6 shows typical X-ray diffraction spectra of the deposited N-doped $SrTiO_3$ films. The pattern of a MgO(100) substrate is shown for comparison. Due to the small film thickness compared to the analysis depth, the spectra reveal a strong (200) reflection of the MgO single crystalline substrate ($2\Theta \sim 42.9°$). A small peak at $2\Theta \sim 38.6°$ also belongs to the MgO(200) reflection due to the Cu K_β X-ray source irradiation line, which was suppressed but not eliminated completely by the diffractometer filter. Analysis of the other reflections shows that all of them belong to the (X00) peak series of strontium titanate. This suggests epitaxial film growth despite the relatively large lattice mismatch (LM) with the substrate, which is defined as:

$$\mathrm{LM} = \frac{a(\mathrm{MgO}) - a(\mathrm{SrTiO_3\ bulk})}{a(\mathrm{SrTiO_3\ bulk})} = +7.8\%\,, \tag{6}$$

where a(MgO) is the unit cell parameter of the MgO substrate (4.211 Å); a($SrTiO_3$ bulk) is the unit cell parameter of the bulk $SrTiO_3$ (3.905 Å). The lattice mismatch is compensated by a tensile strain in the growing film. The relative intensity of the (200) film reflection increases with increasing the laser fluence (Fig. 6) due to an increase of the film thickness.

Most of the studied films reveal epitaxial growth along the (100) plane direction, as described above for the sample series deposited at different laser fluences. However, for the film, deposited at the lowest substrate temperature of 580 °C, an additional (110) reflection was detected in the XRD spectra, indicating a non-oriented growth with poor crystallinity

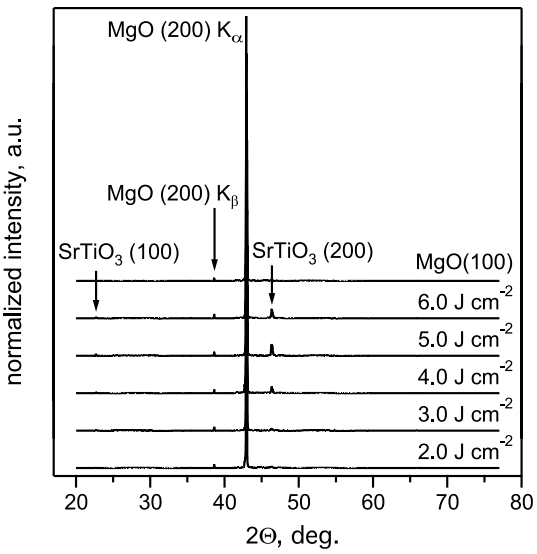

FIGURE 6 XRD patterns of the N-doped $SrTiO_3$ films deposited at various laser fluences at constant $T_{\mathrm{S}} = 650\,^{\circ}\mathrm{C}$ and $d_{\mathrm{T\text{–}S}} = 5.0$ cm. A pattern of a pure MgO substrate (without any film deposited) is included

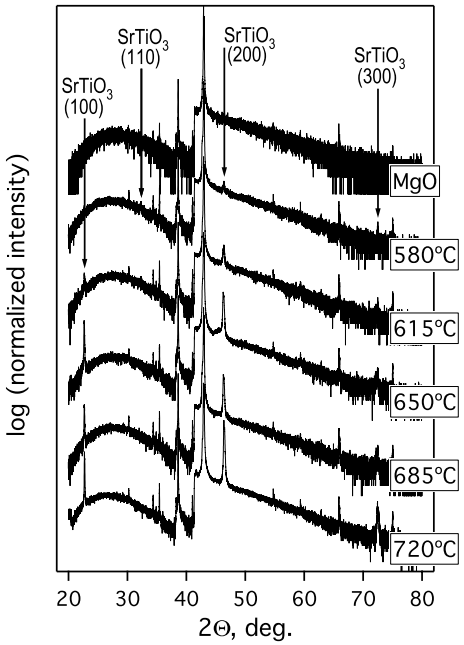

FIGURE 7 XRD patterns of the N-doped $SrTiO_3$ films deposited at various substrate temperatures at constant $F = 5.0\,\mathrm{J\,cm^{-2}}$ and $d_{T\text{-}S} = 5.0\,\mathrm{cm}$. The intensity is plotted in logarithmic scale to enhance the visibility of weak reflections. A pattern of a pure MgO substrate is included

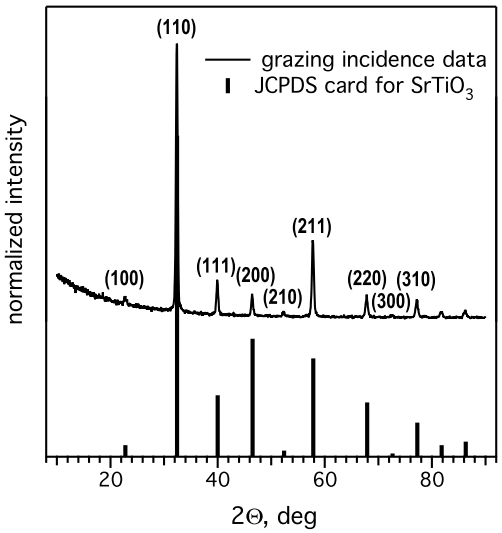

FIGURE 8 Grazing incidence diffraction pattern of a film. All observed reflections are in agreement with those of $SrTiO_3$, confirming the perovskite-type phase purity

and mixed crystallographic orientations (Fig. 7). This clearly indicates that the substrate temperature is determining the crystallographic orientation if the other deposition parameters are constant [24]. An increase of the temperature improves the surface mobility of ions, atoms, and clusters at the substrate, resulting in a higher probability for epitaxial film growth and improved crystallinity. For the substrate temperature of 615 °C the film XRD pattern reveals just a very weak (110) reflection of strontium titanate, while for deposition at higher temperatures (650–720 °C) only epitaxial (100) oriented films with no traces of other orientations are obtained (Fig. 7).

Figure 8 presents a typical XRD pattern of a $SrTiO_3$:N film recorded in the grazing incidence mode. The PDF card for $SrTiO_3$ from the JCPDF database is included as a reference. The XRD pattern reveals a diffraction pattern of polycrystalline strontium titanate due to the small fixed incident angle of the X-rays of 1°. In this case (100) crystallographic planes from the film bulk do not give any diffraction reflections as the Bragg's condition for diffraction maximum is not satisfied. The penetration depth of X-rays at this small incident angle is considerably lower compared to a Θ–2Θ scan. Therefore the film roughness (i.e. topographic features at the film surface) is more important in the grazing incidence XRD, resulting in a diffraction pattern of randomly oriented crystallographic planes. The comparison between the diffraction pattern of the film and the PDF card for pure $SrTiO_3$ unambiguously suggests the formation of a single cubic perovskite-type phase with no traces of impurities.

The unit cell parameters of the studied films, calculated from the XRD data, are presented in Fig. 9 as a function of the film thickness (d). The lattice constants of all $SrTiO_3$:N films are slightly larger compared to bulk strontium titanate due to a number of reasons, such as anionic deficiency of the resulting films [39, 40], N incorporation into the crystal lattice, and a positive lattice mismatch with the substrates. The comparison of the lattice constants of the oxynitride films to the corresponding oxide films (Fig. 9) shows that the oxynitrides have larger unit cell parameters than the corresponding oxides. Therefore, a more precise analysis of the substrate influence on the film lattice constant can be performed by subtracting the increase due to substitution of the smaller oxygen anions in an oxide phase with the larger nitrogen anions in an oxynitride, which can be roughly estimated from the following equation:

$$\frac{a(\text{oxynitride})}{a'(\text{oxide})} \approx \frac{(1-\omega)R(\text{O}) + \omega R(\text{N}) + R(\text{Ti})}{R(\text{O}) + R(\text{Ti})}, \qquad (7)$$

where a(oxynitride) and $a\prime$(oxide) are the unit cell parameter of the oxynitride and the corresponding N-subtracted oxide, respectively; $R(i)$ is the crystallographic radius of the element i ($R(\text{Ti}) = 0.745$ Å, $R(\text{O}) = 1.21$ Å, $R(\text{N}) \approx 1.29$ Å [41]);

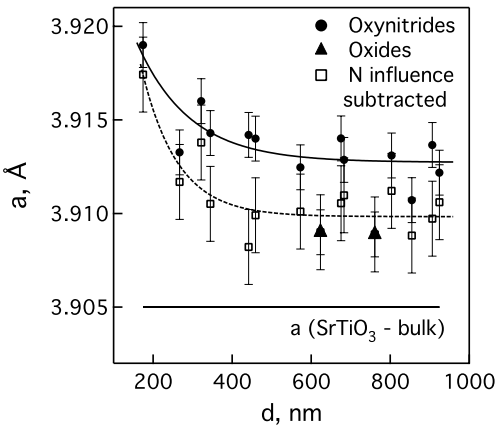

FIGURE 9 The unit cell parameters of the studied films as a function of the film thickness. *Filled circles* guided by a *solid line* represent lattice constants calculated from XRD data. *Open squares* guided by a *dashed line* represent "N influence subtracted" lattice constants (see more details in the text)

ω is the atomic fraction of oxygen substituted with nitrogen in the oxynitride. The resulting subtracted values (a'), shown in Fig. 9 as open squares, are in good agreement with those for oxide films. The unit cell parameters of films with thicknesses below ~ 200–250 nm are higher, compared to others with larger thickness due to the influence of the positive lattice mismatch with the MgO substrates, which is compensated by a tensile strain [40, 42, 43].

4 Conclusions

The deposition parameters and their influence on the composition and crystallinity of oxide films with controlled anionic substitution of O by N have been studied for $SrTiO_3$:N. The thin films were prepared by pulsed reactive crossed beam laser ablation using N_2 for the background and for the gas pulse. Epitaxial perovskite-type films with a roughness of a few nm were deposited on the MgO(100) substrates despite the relatively large lattice mismatch (+7.6%), which is compensated by tensile strain in the films. The unit cell parameters of the $SrTiO_3$:N films are larger compared to bulk $SrTiO_3$ due to the anionic deficiency of the resulting films, N incorporation into the crystal lattice, and a positive lattice mismatch with the substrates. RBS analysis reveals stoichiometric cation transport and oxygen content in the range of $2.70 < [O] < 2.98 \pm 0.15$. This is much higher compared to cobaltate and manganate films deposited by the same technique, suggesting that the oxygen deficiency is strongly influenced by the nature of the deposited material in addition to the deposition parameters. The highest nitrogen content in the studied $SrTiO_3$:N films was obtained for the sample deposited at the highest applied laser fluence of $6.0\,J\,cm^{-2}$, a target-to-substrate distance of 5.0 cm, and a substrate temperature of 650 °C. Below this temperature the formation of the oxynitride phase is kinetically impeded, while heating above 650 °C leads to a decrease of the nitrogen content, probably due to thermodynamical reasons and the lower sticking probability of N compared to O. By varying the deposition parameters (such as laser fluence, target-to-substrate distance, substrate temperature) it is possible to deposit $SrTiO_3$:N films with oxygen and nitrogen contents in the range of $SrTiO_{2.70-2.98}N_{0.030-0.089}$. The presence of an oxidizing source during deposition results in films without any incorporated nitrogen.

ACKNOWLEDGEMENTS We gratefully acknowledge the research group of D. Günther (ETH Zurich) for performing the LA-ICP-MS analysis of the target material. This work is partially supported by MaNEP, Empa and PSI.

REFERENCES

1 L.G. Tejuca, J.L.G. Fierro, *Properties and Applications of Perovskite-Type Oxides* (Marcel Dekker, New York, 1992)
2 R.H. Mitchell, *Perovskites. Modern and Ancient* (Almaz Press, Thunder Bay, Ontario, 2002)
3 F. Tessier, R. Marchand, J. Solid State Chem. **171**, 143 (2003)
4 R. Marchand, F. Tessier, A. Le Sauze, N. Diot, Int. J. Inorg. Mater. **3**, 1143 (2001)
5 Y.I. Kim, P.M. Woodward, K.Z. Baba-Kishi, C.W. Tai, Chem. Mater. **16**, 1267 (2004)
6 D. Yamasita, T. Takata, M. Hara, J.N. Kondo, K. Domen, Solid State Ionics **172**, 591 (2004)
7 I.C. Lekshmi, A. Gayen, M.S. Hegde, Mater. Res. Bull. **40**, 93 (2005)
8 M. Jansen, H.P. Letschert, Nature **404**, 980 (2000)
9 F. Chevire, F. Tessier, R. Marchand, Eur. J. Inorg. Chem. **6**, 1223 (2006)
10 D. Logvinovich, R. Aguiar, R. Robert, M. Trottmann, S.G. Ebbinghaus, A. Reller, A. Weidenkaff, J. Solid State Chem., DOI: 10.1016/j.jssc.2007.06.035 (in press)
11 R. Aguiar, D. Logvinovich, A. Weidenkaff, A. Reller, S.G. Ebbinghaus, Dyes and Pigments **76**, 70 (2008)
12 D. Logvinovich, A. Börger, M. Döbeli, S.G. Ebbinghaus, A. Reller, A. Weidenkaff, Prog. Solid State Chem. **35**, 281 (2007)
13 D.S. Wuu, R.H. Horng, F.C. Liao, C.C. Lin, J. Non-Cryst. Solids **280**, 211 (2001)
14 T. Brauniger, T. Muller, A. Pampel, H.P. Abicht, Chem. Mater. **17**, 4114 (2005)
15 J.S. Horwitz, D.B. Chrisey, R.M. Stroud, A.C. Carter, J. Kim, W. Chang, J.M. Pond, S.W. Kirchoefer, M.S. Osofsky, D. Koller, Appl. Surf. Sci. **129**, 507 (1998)
16 R. Aguiar, D. Logvinovich, A. Weidenkaff, H. Karl, C. Schneider, A. Reller, S.G. Ebbinghaus, Mater. Res. Bull., DOI: 10.1016/j.materresbull.2007.06.049 (in press)
17 L. Le Gendre, C. Le Paven, J. Pinel, D. Fasquelle, J.C. Carru, F. Chevire, F. Tessier, R. Marchand, Silicates Industriels **69**, 165 (2004)
18 Y. Cohen, I. Riess, Mater. Sci. Eng. B **25**, 197 (1994)
19 G. Rijnders, D.H.A. Blank, Nature **433**, 369 (2005)
20 J.S. Horwitz, D.B. Chrisey, P.C. Dorsey, L.A. Knauss, J.M. Pond, M. Wilson, M.S. Osofsky, S.B. Qadri, J. Caulfield, R.C.Y. Auyeung, Nucl. Instrum. Methods Phys. Res. B **121**, 371 (1997)
21 M. Miyauchi, M. Takashio, H. Tobimatsu, Langmuir **20**, 232 (2004)
22 P.R. Willmott, R. Timm, J.R. Huber, J. Appl. Phys. **82**, 2082 (1997)
23 P.R. Willmott, Prog. Surf. Sci. **76**, 163 (2004)
24 T. Lippert, in: *Photon-based Nanoscience and Nanobiotechnology*, ed. by J.J. Dubowski, S. Tanev (Springer, Amsterdam, 2006), p. 267
25 M.J. Montenegro, C. Clerc, T. Lippert, S. Muller, P.R. Willmott, A. Weidenkaff, A. Wokaun, Appl. Surf. Sci. **208**, 45 (2003)
26 S. Canulescu, T. Lippert, H. Grimmer, A. Wokaun, R. Robert, D. Logvinovich, A. Weidenkaff, A. Doebeli, Appl. Surf. Sci. **252**, 4599 (2006)
27 D. Bäuerle, *Laser Processing and Chemistry*, 3rd ed. (Springer, Berlin, 2000)
28 M.J. Montenegro, T. Lippert, in: *Pulsed Laser Deposition of Thin Films*, ed. by R.W. Eason (Wiley, New York, 2007), p. 563
29 M.J. Montenegro, K. Conder, M. Dobeli, T. Lippert, P.R. Willmott, A. Wokaun, Appl. Surf. Sci. **252**, 4642 (2006)
30 *Dektak 8 Advanced Development Profiler Manual* (Veeco Instruments, 2004)
31 W.K. Chu, J.W. Mayer, M.A. Nicolet, *Backscattering Spectrometry* (Academic Press, New York, London, 1978)
32 L.R. Doolittle, Nucl. Instrum. Methods Phys. Res. B **15**, 227 (1986)
33 R. Perez-Casero, J. Perriere, A. Gutierrez-Llorente, D. Defourneau, E. Millon, W. Seiler, L. Soriano, Phys. Rev. B: Condens. Matter **75**, 165 317 (2007)
34 A. Schmehl, F. Lichtenberg, H. Bielefeldt, J. Mannhart, D.G. Schlom, Appl. Phys. Lett. **82**, 3077 (2003)
35 S. Canulescu, G. Dinescu, G. Epurescu, D.G. Matei, C. Grigoriu, F. Craciun, P. Verardi, M. Dinescu, Mater. Sci. Eng. B **109**, 160 (2004)
36 P.J. Gellings, H.J.M. Bouwmeester, *The CRC Handbook of Solid State Electrochemistry* (CRC Press, Boca Raton, 1997)
37 J.B. Malherbe, S. Hofmann, J.M. Sanz, Appl. Surf. Sci. **27**, 355 (1986)
38 K. Sturm, H.U. Krebs, J. Appl. Phys. **90**, 1061 (2001)
39 S. Miyoshi, J.O. Hong, K. Yashiro, A. Kaimai, Y. Nigara, K. Kawamura, T. Kawada, J. Mizusaki, Solid State Ionics **161**, 209 (2003)
40 C. Wang, B.L. Cheng, S.Y. Wang, H.B. Lu, Y.L. Zhou, Z.H. Chen, G.Z. Yang, Thin Solid Films **485**, 82 (2005)
41 R.D. Shannon, Acta Cryst. A **32**, 751 (1976)
42 R. Kalyanaraman, R.D. Vispute, S. Oktyabrsky, K. Dovidenko, K. Jagannadham, J. Narayan, J.D. Budai, N. Parikh, A. Suvkhanov, Appl. Phys. Lett. **71**, 1709 (1997)
43 F.Z. He, B.O. Wells, S.M. Shapiro, Phys. Rev. Lett. **94** (2005)